

# Journal of

# **Applied and Computational Mechanics**



Research Paper

# Effect of Initial Conditions on the Behavior of Two-Electrode MEMS with Variable Interelectrode Gap

Valery P. Dragunov<sup>1</sup>, Dmitriy I. Ostertak<sup>1</sup>, Evgeniya V. Dragunova<sup>2</sup>, Maksim A. Kuznetsov<sup>1</sup>

Department of Semiconductor Devices and Microelectronics, Novosibirsk State Technical University, Novosibirsk 630073, Russia, Email: dragunov@corp.nstu.ru (V.P.D.); ostertak@corp.nstu.ru (D.I.O.); m.kuznetsov@corp.nstu.ru (M.A.K.)

Received June 8 2025; Revised September 13 2025; Accepted for publication September 26 2025.

☐ Corresponding author: D.I. Ostertak (ostertak@corp.nstu.ru)

© 2025 Published by Shahid Chamran University of Ahvaz

Abstract. The influence of initial conditions on the behavior of two-electrode microelectromechanical systems (MEMS) having parallel-plate and comb structures with variable interelectrode gap is studied and analyzed here within a nonlinear approach. It has been revealed that the two-electrode MEMS operation is considerably influenced not only by the initial conditions and the system characteristics, but also the speed of the applied electrical voltage change. It has been established that during slow change of the applied voltage the constant force along with the nonlinear restoring force can lead to emergence of the second unstable equilibrium point on the dependences of the movable electrode displacement versus the applied voltage. As a result, when the applied voltage reverses a hysteresis can occur in the system. It is shown that due to the optimal use of the constant force in MEMS with the nonlinear dependence of the restoring force versus the movable electrode displacement, the capacitance modulation depth and the relative range of the controlled capacitance change can be increased by several times in comparison with MEMS having the linear dependence of the restoring force. Analytical formulas have been obtained to get separatrices defining the set of initial conditions for which periodic oscillations are observed in case of MEMS excitation using a voltage step. It is demonstrated that for MEMS with the comb structure of electrodes where not only the fixed, but also the movable electrode is split, the pull-in voltage decreases when the number of the split electrode components increases.

Keywords: Electrostatic force, Nonlinearity, Capacitance modulation, Static equilibrium, Separatrix.

# 1. Introduction

One of the most prevailing methods of actuation used in microelectromechanical systems (MEMS) is electrostatic actuation. To date, many different electrostatic MEMS have been developed, which are used in various fields of human activity [1–14]. Electrostatic actuation is also suitable for creating vibration energy harvesters which can be used as alternative power sources in wireless sensor networks [15–17].

An applied voltage between the electrodes of devices based on electrostatic MEMS generates the Coulomb force of attraction [18, 19]. This force makes the electrode to move resulting in a change of capacitance. The electrostatic force is inversely proportional to the square of the interelectrode gap and increases quadratically with its decreasing. For many applications a larger displacement of the electrode is desirable because it increases the range of capacitance change. However, as the range of electrode movement increases by decreasing the interelectrode gap, the electrostatic force acting between the electrodes grows and can exceed at a certain moment the mechanical restoring force, leading to the pull-in effect between the electrodes [18–27]. Thus, the range of the electrode movement for MEMS becomes limited.

The analysis of the pull-in effect typically falls into two categories: quasi-static and dynamic. Quasi-static models [19–28] assume slow voltage changes, neglecting inertial effects, and are suitable for analyzing the final stages of pull-in effect. Dynamic models [29–43], conversely, explicitly incorporate the system's inertia and transient response. These analyses, often employing numerical techniques, are crucial for understanding the entire pull-in process, including the time-dependent trajectory of the movable electrode and the impact of initial conditions. As demonstrated in previous works [30, 33, 34, 36–38] the initial displacement and velocity of the movable electrode can significantly influence to the pull-in voltage and time dependences of the electrode displacement.

The features of the operation of two-electrode MEMS with variable interelectrode gap under arbitrary initial conditions, taking into consideration the electromechanical interactions and inertial properties of the system with a very slow (quasi-static) change of the applied voltage have been studied and analyzed in [37, 38].

In this paper, the influence of the parameters of two-electrode MEMS with interelectrode gap change and their state immediately before applying electrical excitation on the operation of such systems is analyzed, taking into consideration the constant force and electromechanical coupling within a nonlinear approximation for the restoring elastic and electrostatic forces.



<sup>&</sup>lt;sup>2</sup> Department of Computer Science in Economics, Novosibirsk State Technical University, Novosibirsk 630073, Russia, Email: dragunova@corp.nstu.ru

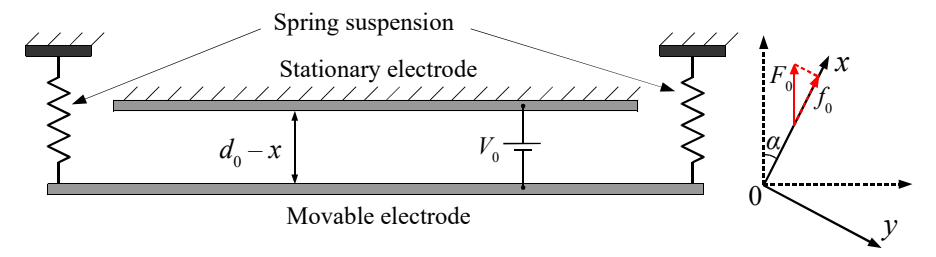


Fig. 1. Simplified model of the analyzed electromechanical system.

#### 2. The Model

Let's analyze the main peculiarities of the two–electrode MEMS behavior with the simplified model of the electromechanical system illustrated in Fig. 1, comprising the stationary and movable electrodes, as well as elastic suspensions, here  $V_0$  is the voltage applied between the movable and stationary electrodes,  $d_0$  is the initial gap between the electrodes (without external forces action), x is the movable electrode displacement relative to its initial position.

The movable electrode of MEMS experiences several forces: the elastic restoring force, the electrostatic attractive force, and the constant external force  $F_0$  (for example, gravity). The value of the force  $F_0$  projection to the surface normal of the movable element  $f_0$  can vary from  $-F_0$  to  $F_0$  depending on the MEMS orientation. It is necessary to note that the rate of the applied voltage  $V_0$  change can significantly vary during the MEMS excitation.

Modern fabrication techniques, employing integrated circuit processes, enable the creation of MEMS with exceptionally high-quality factors (Q-factor). In order for the Q-factor to be greater than 100 the system must be evacuated. Values reaching tens of thousands are reported in the literature [44, 45], indicating minimal energy dissipation during oscillations. This high Q-factor allows for sustained oscillations over many cycles.

Analyzing the behavior of the system immediately after its launch it is possible to confine only with consideration of an initial short time interval lasting only a few periods of the system's natural oscillations, when dissipative processes don't have any significant contribution.

The equation of motion, incorporating the nonlinear spring force, can be expressed as a forced Duffing equation without damping [31, 33, 46]:

$$m\frac{d^2x}{dt^2} = -kx - k_3x^3 + \frac{\varepsilon_0\varepsilon S}{2} \left(\frac{V_0}{d_0 - x}\right)^2 + F_0\cos(\alpha), \tag{1}$$

where m is the mass of the movable electrode, k is the linear spring constant,  $k_3$  is the coefficient characterizing the cubic nonlinearity of the restoring force,  $\varepsilon_0$  is the permittivity of free space,  $\varepsilon$  is relative permittivity of the gas within the interelectrode gap, S is the area of the electrode overlap,  $\alpha$  is the angle between the direction of the normal to the movable electrode surface and the direction of the external force  $F_0$ .

It should be noted that Eq. (1) does not take into account the nonuniformity of electric field within the interelectrode gap (fringing field effects). However, the estimations [47] show that for  $(d_0 - x)/S^{0.5} < 0.02$  the capacitance can be determined using ideal parallel-plate capacitor formula with an error less than 10%. In addition, it is necessary to take into account that the electric field strength within the interelectrode gap should not exceed the breakdown value, which, for example, for air is 30 kV/cm.

By introducing dimensionless variables Eq. (1) can be represented as:

$$\frac{d^2z}{d\tau^2} = -z - \beta z^3 + \frac{\lambda}{(1-z)^2} + F,$$
(2)

where  $\lambda = C_0 V_0^2 / (2kd_0^2)$  is the dimensionless voltage,  $z = x/d_0$  is the relative displacement of the movable electrode,  $\beta = k_3 d_0^2/k$ ,  $C_0 = \varepsilon_0 \varepsilon S / d_0$ ,  $\tau = \omega_0 t$ ,  $\omega_0 = \sqrt{k/m}$  and  $F = F_0 \cdot \cos(\alpha) / (kd_0)$  is the normalized projection of the constant force. The value of F can be varied by changing both  $F_0$  and  $\alpha$ .

Therefore, taking into consideration the constant force, the behavior of the analyzed two-electrode system within the nonlinear approximation is determined by three parameters  $\lambda$ ,  $\beta$  and F.

# 3. MEMS Operation Analysis

#### 3.1. Quasi-static approximation

First of all, let's analyze the behavior of MEMS under constant or very slowly changing influences – a quasi-static approximation (the first limiting case). This situation can be realized, for example, during micro tweezers and tunable microcapacitors operation. In this case, the initial condition is the interelectrode gap value at the moment when the excitation voltage is applied. This gap can change before the excitation moment if the MEMS spatial orientation and the value of residual charge on the electrodes change.

In this case, one can ignore the term  $d^2z/d\tau^2$  in Eq. (2). We will also assume that at the time when the voltage  $V_0$  is applied, no additional external forces act on the movable electrode, and there are no residual charges on the electrodes. As a result, during the system startup, the velocity of the movable electrode  $v_{\text{init}} = dz_{\text{init}}/d\tau$  is zero, and the displacement  $z_{\text{init}}$  is determined by the following ratio:

$$z_{init} + \beta z_{init}^3 = F.$$

For this approximation, the equilibrium equation linking the parameter  $\lambda$  and the coordinate of the static equilibrium position  $z_0$  can be represented as:

$$\Phi(z_0, \lambda, \beta) = (z_0 + \beta z_0^3 - F)(1 - z_0)^2 - \lambda = 0.$$
(3)



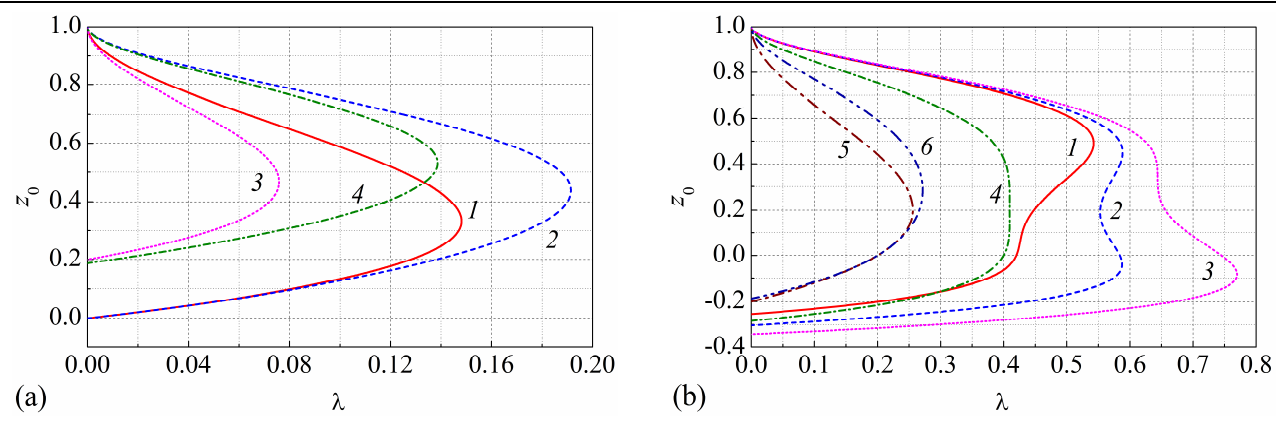


Fig. 2. Dependences of the static equilibrium position  $z_0$  versus the magnitude of the dimensionless voltage  $\lambda$  calculated for different values of F and  $\beta$ : (a) for  $F \ge 0$ , and (b) for F < 0.

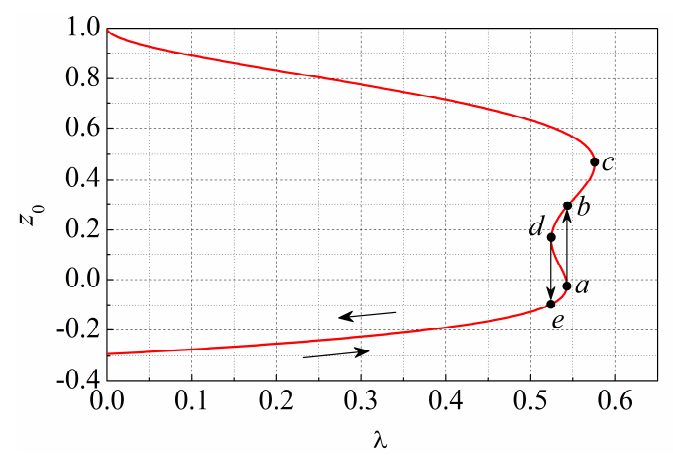


Fig. 3. The dependence of the static equilibrium position on the magnitude of the dimensionless voltage  $\lambda$  at  $\beta$  = 10, F = -0.542.

Figure 2 shows the dependences of the static equilibrium position  $z_0$  of the movable electrode versus the magnitude of the dimensionless voltage  $\lambda$  calculated using Eq. (3) for several values of the MEMS parameters  $\beta$  and F: a) for  $F \ge 0$ ,  $\beta = 0$ , F = 0 (curve 1);  $\beta = 2$ , F = 0 (curve 2);  $\beta = 0$ , F = 0.2 (curve 3);  $\beta = 2$ , F = 0.2 (curve 4); and b) for F < 0,  $\beta = 10$ , F = -0.42 (curve 1);  $\beta = 10$ , F = -0.42 (curve 3);  $\beta = 5$ , F = -0.42 (curve 4);  $\beta = 0$ , F = -0.22 (curve 5);  $\beta = 2$ , F = -0.22 (curve 6). It can be seen that in the case when the force  $F_0$  tends to reduce the interelectrode gap (F > 0), there is one extremum (point of unstable equilibrium) on these dependences, which characterized by the values of the relative displacement  $z_{cr}$  and the dimensionless voltage  $\lambda_{cr}$ , and an increase of  $\beta$  and F leads to an increase of  $z_{cr}$  and  $z_{cr}$ . It should be noted that the parts of the curves shown in Fig. 2 corresponding to  $z \ge z_{cr}$  represent the points of unstable equilibrium.

According to Fig. 2(a) when F > 0, at a slow (quasi-static) increase of the applied voltage, the interelectrode gap will decrease monotonously. If now, before reaching  $\lambda_{cr}$  we start to decrease  $\lambda$ , then the decrease of  $z_0$  will occur according to the same trajectory as when increasing  $\lambda$ , but in reverse order. If, during an increase of the applied voltage, the magnitude of the dimensionless voltage  $\lambda$  reaches the value of  $\lambda_{cr}$ , then with a further increase of the applied voltage, the interelectrode gap will uncontrollably begin to decrease at the maximum possible speed until the movable electrode comes into a contact with the stationary one causing the electrodes collapse (pull-in instability effect). After that, the movable and stationary electrodes will remain pressed against each other even when the applied voltage decreases below the critical one. In this case, the movable electrode will detach from the stationary one and return to its original position only when the applied voltage reaches zero.

In the case when the force  $F_0$  tends to increase the interelectrode gap (F < 0) (e.g., when the spatial orientation of the MEMS has changed) an additional extremum can appear on the dependences  $z_0(\lambda)$  (Fig. 2(b)). That is for negative F, two critical points (two extrema) are possible, which characterized by values of the relative displacement  $z_{cr,1}$  and  $z_{cr,2}$ , as well as dimensionless voltages  $\lambda_{cr,1}$  and  $\lambda_{cr,2}$ . Both of these points are points of unstable equilibrium. It should be noted that the regions of the curves shown in Fig. 2 where  $dz/d\lambda \le 0$  correspond to the states of unstable equilibrium.

If, for certain system parameters one extremum is realized on the dependences  $z_0(\lambda)$ , then the behavior of the system at F < 0 will be similar to the behavior of the system at F > 0. If, at the given parameters, two extrema are realized on the dependences  $z_0(\lambda)$ , then a hysteresis can be observed during the reversible change of the applied voltage (Fig. 3).

Such behavior of the system can be explained by the fact that at negative values of  $z_0$  the return and electrostatic forces are directed in one direction (toward the stationary electrode) and both forces tend to return the system to the neutral position, which was established before the influence by the force  $F_0$  (F < 0). During transition from point "a" to point "b" the electrostatic force does not change the direction, but the returning force at  $z_0 > 0$  reverses its direction and increases rapidly (non-linearly) acting against the electrostatic force along with  $F_0$ . At the same time, equilibrium is also achieved at point "b".

As a result, during the slow increase of the control voltage  $\lambda$ , the movable electrode displacement  $z_0$  will first decrease monotonously (Fig. 3) until it reaches the critical point "a", then the displacement of  $z_0$  will change sharply to the value corresponding to point "b", and then continues to change monotonously to the second critical point (point "c"). In this case, a further increase of  $\lambda$  will lead to an uncontrolled motion of the movable electrode to the stationary one until the electrodes come into contact (pull-in effect).



If, before reaching the critical point "c", one starts to reduce  $\lambda$ , then the reverse jump of the movable electrode will occur at values  $z_0$  and  $\lambda$  corresponding to the point "d". As a result, dependences of the movable electrode position versus the applied voltage during changing the direction of the voltage variation will not coincide, and some hysteresis will be observed here. Such hysteresis enables to eliminate the chattering of the movable electrode at voltages close to  $\lambda_a$ , which occurs due to fluctuations of the applied voltage (e.g., due to the noise influence).

The presence of the linear component for the returning force reduces this effect. Therefore, the features inherent for a particular system may be related to the shape of elastic suspensions and electrodes, the stiffness of the system and its other design parameters.

According to Eq. (3), for taking into account the nonlinearity of elastic suspensions and the force  $F_0$ , the dependence of the critical displacement  $z_{cr}$  versus  $\beta$  and F is determined by Eqs. (4) and (5):

$$Z_{cr,1}(\beta,F) = A_1(\beta,F) + A_2(\beta,F) + 0.2,$$
 (4)

$$Z_{cr,i}(\beta,F) = -0.5(A_1(\beta,F) + A_2(\beta,F)) \pm j0.5\sqrt{3}(A_1(\beta,F) - A_2(\beta,F)) + 0.2,$$
(5)

where  $i = 2, 3, \beta > 0, F < 1, and,$ 

$$A_{1,2}(\beta,F) = \sqrt[3]{\frac{0.008}{\beta} \left(5 + 25F + \beta \pm 5\sqrt{\frac{5 - 2\beta + \beta^2 + (10 + 25F + 2\beta)\beta F}{\beta}}\right)}.$$

Equations (4) and (5) defining the coordinates of the critical points (i.e., the three extrema on the curves shown in Fig. 2) are obtained using Eq. (3) by differentiation of  $\lambda$  with respect to the coordinate z and equating the result to zero. As a result, a cubic equation is obtained, which solutions determine the desired coordinates.

Figure 4 shows the dependences of the critical points position versus the dimensionless force F calculated using Eqs. (4) and (5) for different values of  $\beta$ . Solid lines are for dependences  $z_{cr.1}$ , dashed lines are for  $z_{cr.2}$ , and dotted lines are for  $z_{cr.3}$ .

An analysis of Eqs. (4), (5) and Fig. 4 shows the following features: 1) the values of  $z_{cr,1}$  and  $z_{cr,2}$  defines the coordinates of the critical points "c" and "a" (Fig. 3), whereas  $z_{cr,3}$  defines the coordinate of the minimum between them (point "d" in Fig. 3); 2) for dimensionless force F = 0.4 the coordinate of the critical point "c" does not depend on the value of  $\beta$  (nonlinear degree) and equals 0.6; 3) the second maximum arises only if  $\beta > 5$  and F < -0.4; 4) one can observe two maxima on the dependences  $z_0(\lambda)$  if for the given  $\beta$  the value of F will be varied from  $F_{min}$  to  $F_{max}$ , where

$$F_{\min} = -\frac{0.04}{\beta} \left[ \sqrt{\beta (\beta - 5)^3} + 5\beta + \beta^2 \right], \quad F_{\max} = \frac{0.04}{\beta} \left[ \sqrt{\beta (\beta - 5)^3} - 5\beta - \beta^2 \right]. \tag{6}$$

Figure 5 shows the dependences of  $F_{max}$  and  $F_{min}$  versus  $\beta$ . At the system parameters for which  $\beta$  and F are in the region limited by these curves two maxima will be observed on the dependences  $z_0(\lambda)$ . Equations (4) and (5) also enable to calculate the dependences of achievable capacitance modulation depth  $\eta = C_{max}/C_{min}$  and the relative range of the controlled capacitance change  $\eta_d = 2(C_{max} - C_{min})/(C_{max} + C_{min})$  versus the dimensionless force F during the applied voltage change. These parameters determine the efficiency of MEMS tunable capacitors and the influence of the MEMS spatial orientation and the movable electrode weight on these capacitors. The corresponding dependences are shown in Figs. 6 and 7, respectively.

The main feature of these dependences is the presence of the maxima. As the value of  $\beta$  increases the position of the maxima is shifted towards the negative values of F, whereas the values of  $\eta$  and  $\eta_d$  grow. It should be noted that using the linear approximation for the returning force the values of  $\eta$  and  $\eta_d$  do not depend on the movable electrode weight and are equal to 1.5 and 0.4, respectively. While as the nonlinearity of the mechanical system increases the values of  $\eta$  and  $\eta_d$  start to change during the change of the movable electrode weight.

Figure 8 shows the dependences of the maximum achievable capacitance modulation depth  $\eta_{\text{max}}$  and the relative range of the controlled capacitance change  $\eta_{d,\text{max}}$  versus the value of  $\beta$ . For  $\beta \leq 10$  it is possible to approximate these dependences with 2% error by the following formulas:

$$\eta_{\text{max}} = 1.5 + 0.156\beta - 0.0057\beta^2, \quad \eta_{d,\text{max}} = 0.4 + 0.086\beta - 0.004\beta^2.$$

It is obvious that using an optimal weight of the movable electrode in MEMS with nonlinear behavior of the returning force the capacitance modulation depth and the relative range of the controlled capacitance change can be increased by several times in comparison with MEMS having linear dependence of the returning force on the movable electrode displacement.

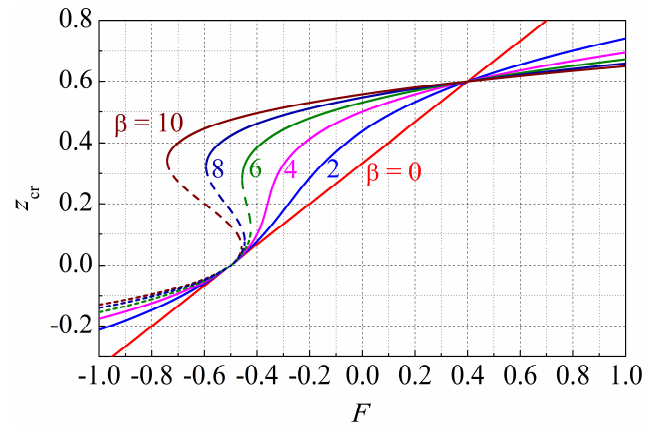
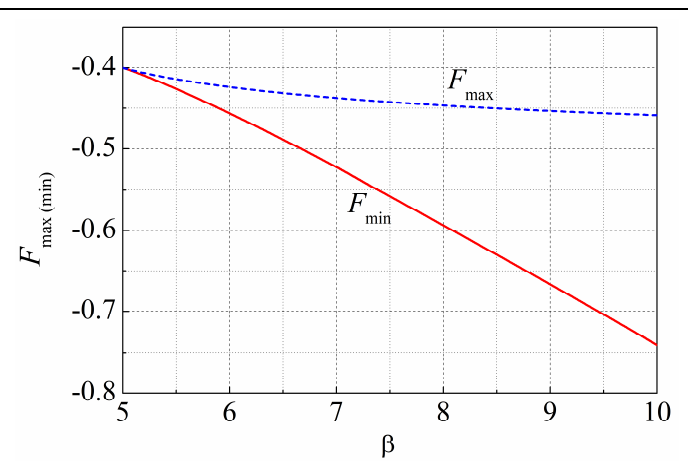


Fig. 4. Dependences of the critical points position versus dimensionless force F. The curve number indicates the value of parameter  $\beta$ .





**Fig. 5.** Dependences of  $F_{max}$  and  $F_{min}$  versus  $\beta$ .

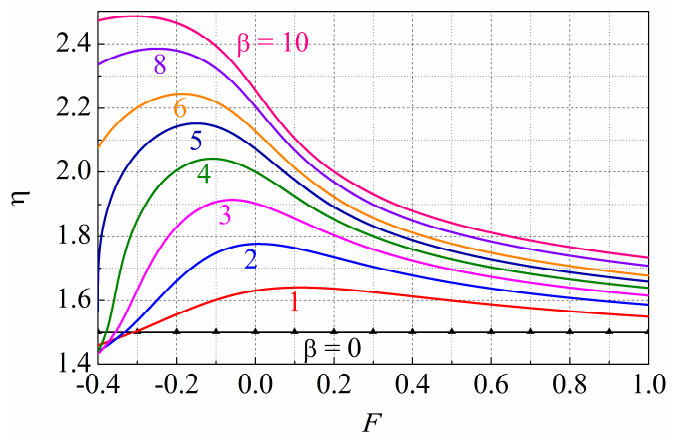


Fig. 6. The achievable capacitance modulation depth dependence versus the dimensionless force for different values of  $\beta$ .

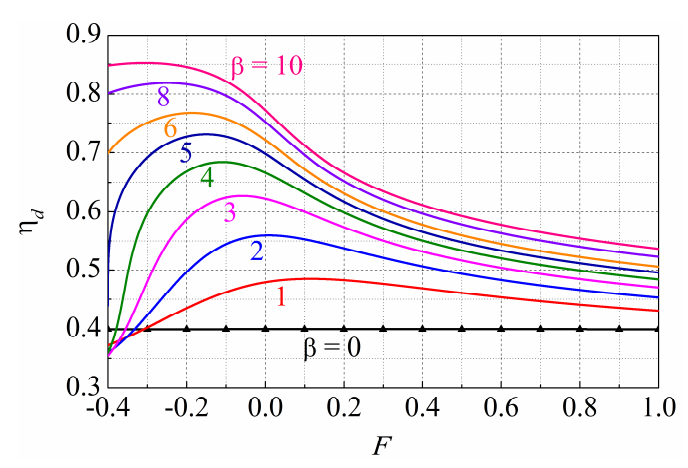


Fig. 7. The dependence of the relative range of the controlled capacitance changes versus the dimensionless force for different values of  $\beta$ .

It also follows from the static equilibrium condition described by Eq. (3) that the system will remain controllable (no pull-in effect) if for defined values  $\beta$  and F the value of  $\lambda$  will be less than

$$\lambda_{\rm cr} = (z_{\rm cr} + \beta z_{\rm cr}^3 - F)(1 - z_{\rm cr})^2,$$
 (7)

and the applied voltage  $V_0$  will not exceed the value of:

$$V_{0,\rm cr} = \sqrt{\frac{2kd_0^2}{C_0}(z_{\rm cr} + \beta z_{\rm cr}^3 - F)(1 - z_{\rm cr})^2}.$$

It should be noted that for given  $\beta$  and  $F_0$  the values of  $\lambda_{cr}$  and  $d_0$  strongly depend on spatial orientation of MEMS, which is necessary to take into account during MEMS design and can be used for initial interelectrode gap  $d_0$  adjustment without any external force. Figure 9 shows the dependences of  $\lambda_{cr}$  versus the angle  $\alpha$  calculated for different values of the restoring force nonlinearity  $\beta$ . The breaks on the dependences appear when the values of  $F(\alpha)$  become less than the value of  $F_{min}$  corresponding to the specified  $\beta$ .



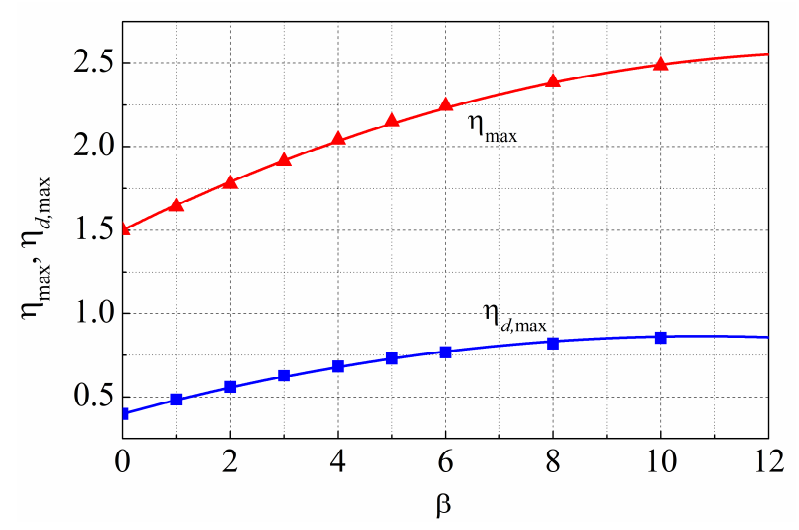


Fig. 8. Dependences of the maximum achievable capacitance modulation depth  $\eta_{\text{max}}$  and the relative range of the controlled capacitance change  $\eta_{\text{d.max}}$  versus the value of  $\beta$ .

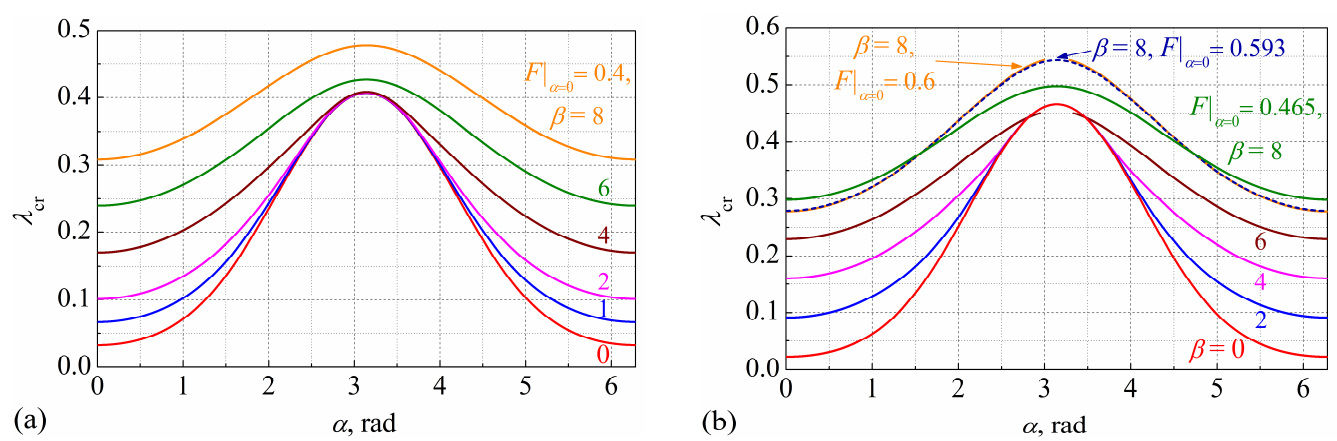


Fig. 9. Dependences of  $\lambda_{cr}$  versus the angle  $\alpha$  calculated for different  $\beta$ :  $F(\alpha = 0) = 0.4$  (a),  $F(\alpha = 0) = 0.465$ , 0.593 and 0.6 (b).

It is obvious from Fig. 9 that the variation of the movable electrode orientation can change the value of  $\lambda_{cr}$  by several times. These dependences also enable to evaluate the change of MEMS parameters fixed on slowly swinging objects, such as television masts.

It has been analyzed that if MEMS has orientation corresponding to  $\alpha=\pi/2$  then for two-electrode system with "linear" spring suspensions ( $k\neq0$ ,  $k_3=0$ )  $z_{cr}=1/3$ , and  $V_{0,cr}=\sqrt{0.296kd_0^2/C_0}$ . Whereas for "nonlinear" spring suspensions (k=0,  $k_3\neq0$ ) the corresponding values in case of  $\alpha=\pi/2$  are  $z_{cr}=3/5$ , and  $V_{0,cr}=\sqrt{0.0691k_3d_0^4/C_0}$ . This is consistent with the results of [18, 31, 48] without a constant force independent on the displacement of the movable electrode. Thus, the use of two-electrode MEMS with a nonlinear restoring force can increase the range of the movable electrode controlled displacement by 1.8 times. As a result, for example, the range of capacitance changes in tunable MEMS capacitors can be significantly increased.

In some cases, two-electrode MEMS with a comb structure of electrodes and a split fixed electrode are used in electronic devices [49]. For this design, the movable electrode can move between two components of the split stationary electrode, which are mechanically and electrically connected to each other as shown in Fig. 10. In this case, the value of  $d_0$  will be equal to half of the distance between the stationary electrode components.

As a rule, such MEMS are oriented with the angle  $\alpha = \pi/2$ . Without damping the equilibrium equation for such a system can be represented as:

$$m\frac{d^2x}{dt^2} = -kx - k_3x^3 + \frac{\varepsilon_0\varepsilon S}{2} \left[ \left(\frac{V_0}{d_0 - x}\right)^2 - \left(\frac{V_0}{d_0 + x}\right)^2 \right].$$

Visually this equation coincides with Eq. (1). Therefore, the conditions of applicability of this equation are the same as for Eq. (1). In dimensionless variables the equilibrium equation (similar to Eq. (2)) for MEMS with a comb structure of electrodes takes the form:

$$\frac{d^2z}{d\tau^2} = -z - \beta z^3 + \frac{4\lambda z}{(1-z^2)^2}.$$
 (8)

In these terms, the behavior of the system is determined by two parameters,  $\lambda$  and  $\beta$ , and the equilibrium equation linking the value of  $\lambda$  with the coordinate of the static equilibrium position  $z_0$  can be expressed as:

$$\Phi(z_0, \lambda, \beta) = (1 + \beta z_0^2)(1 - z_0^2)^2 - 4\lambda = 0.$$
(9)



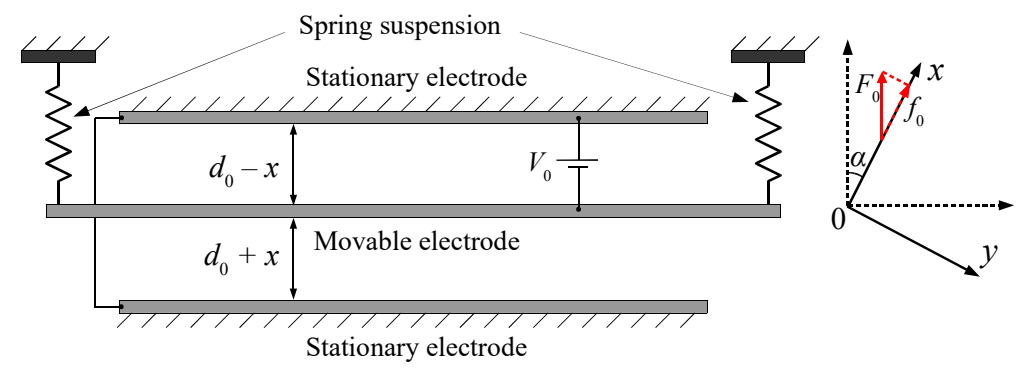


Fig. 10. Simplified model of the MEMS with a split fixed electrode.

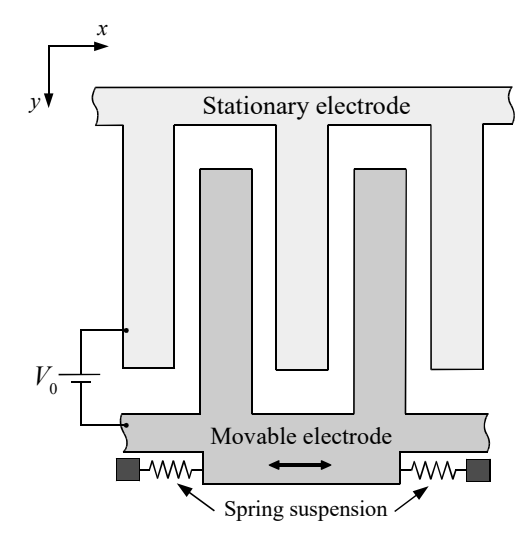


Fig. 11. Simplified model of the MEMS with split fixed and stationary electrodes.

The analysis shows that as the value of  $\beta$  increases from 0 to 2 the changes of the dependences  $z_0(\lambda)$  are only quantitative, but for  $\beta > 2$  there are also qualitative changes. It follows from the condition of static equilibrium described by Eq. (9) that at  $\beta > 2$  the system will remain controllable if the value of  $\lambda$  is less than:

$$\lambda_{\rm cr} = \frac{1}{27\beta^2} (\beta + 1)(\beta - 1)^2,$$
 (10)

and the applied voltage V<sub>0</sub> does not exceed the value of:

$$V_{\rm 0,cr} = \sqrt{\frac{2kd_{\rm 0}^2}{27C_{\rm 0}}(\beta+1)\!\!\left(1-\frac{1}{\beta}\right)^2}\,.$$

According to Eq. (9) when such voltage is applied in the static case the displacement of the movable electrode will be equal to:

$$|\mathbf{z}_{\rm cr}| = \sqrt{\frac{\beta - 2}{3\beta}}.$$

As the value of  $\beta$  increases the value of  $|z_{cr}|$  tends to  $1/\sqrt{3}$ . Thus, for this MEMS design the range of controlled displacement of the movable electrode will extend from 0 to  $d_0/\sqrt{3}$ , which is greater than the corresponding range for MEMS with "linear" elastic suspensions.

For most cases, two-electrode MEMS with a comb structure of electrodes are used in electronic devices, where not only stationary, but also movable electrode is split as shown in Fig. 11. For this design, the n components of the split movable electrode move between the n+1 components of the split stationary electrode. The components of each electrode are mechanically and electrically interconnected.

The equilibrium equation for MEMS with a comb structure of electrodes (containing 2n + 1 components) where not only a fixed, but also a movable electrode is split takes the form of Eq. (8), where it is necessary to use  $\lambda^* = n \cdot \lambda$  instead of  $\lambda$ . Taking into account such a replacement, all other equations and conclusions obtained for two-electrode MEMS with a comb structure of electrodes and with only a fixed split electrode will be correct.

#### 3.2. Dynamic excitation

In addition to the quasi-static change of the applied voltage the dynamic excitation is often observed during the operation of MEMS, when a change of the system state occurs under the impact of a rapidly changing electrical voltage. The limiting case is a voltage surge in the form of a step (the second limiting case). In this case, the initial conditions are the values of the interelectrode gap, the initial velocity, and the value of residual charge on the electrodes, which could alter at the end of previous



processes, and must be pre-determined at the moment when the excitation voltage is applied. Here, depending on the initial parameters, either periodic oscillations or pull-in of the electrodes can be observed. Moreover, for the normal operation of some MEMS (e.g., microgenerators) it is required to have the oscillating mode, and for others (e.g., microrelays) it is necessary to get the contact between the electrodes.

The behavior analysis of the two-electrode nonlinear MEMS described by Eq. (2) under the influence of a voltage surge in the form of a step will be conducted using the phase trajectories [50]. It is necessary to take into account that the movable electrode initial velocity  $v_{\text{init}}$  and displacement  $z_{\text{init}}$  could be non-zero.

Let's take Eq. (2) as a system of two differential equations:

$$\frac{dz}{d\tau} = v$$
,  $\frac{dv}{d\tau} = -z - \beta z^3 + \frac{\lambda}{(1-z)^2} + F$ .

Taking into account that  $d\tau = dz/v$  and using the method of separation of variables the second equation can be represented as:

$$vdv = \left(-z - \beta z^3 + \frac{\lambda}{(1-z)^2} + F\right)dz.$$

By integrating the last equation, the integral curves in the phase plane can be represented as

$$v^2 = 2Fz - z^2 - \frac{\beta}{2}z^4 + \frac{2\lambda}{(1-z)} + \text{const.}$$
 (11)

Here, the separatrix equation taking into account the symmetry of the problem can be as follows

$$v = \pm \sqrt{2F - (z+b) - \frac{\beta}{2}(z^2 + b^2)(z+b) + \frac{2(b+\beta b^3 - F)(1-b)}{(1-z)}} | (z-b),$$
(12)

where b is the coordinate of a special point of the saddle type corresponding to the maximum allowed controlled distance between the movable and fixed electrodes.

It is necessary to note that for a given value of b the separatrix corresponds to the voltage step of:

$$\lambda = (b + \beta b^3 - F)(1 - b)^2. \tag{13}$$

The analysis of Eq. (12) showed that the behavior of MEMS can significantly change depending on the location of the system parameters  $\beta$  and F relative to the area bounded by the curves  $F_{max}$  and  $F_{min}$  (Fig. 5).

Figure 12(a) represents separatrices calculated for MEMS with different values of  $\beta$ , F,  $\lambda$ :  $\beta$  = 0, F = 0,  $\lambda_1$  = 0.119808,  $z_{cr}(\lambda_1)$  (curve 1);  $\beta$  = 2, F = 0,  $\lambda_2$  =  $\lambda_1$ ,  $z_{cr}(\lambda_2)$  (curve 2);  $\beta$  = 0, F = 0.2,  $\lambda_3$  = 0.06,  $z_{cr}(\lambda_3)$  (curve 3), and initial conditions ( $z_{init}$  = 0.9999992 $z_{cr}$ ,  $v_{init}$  = 0), also the corresponding time dependences of the movable electrode displacement are shown in Fig. 12(b). Here  $z_{cr}$  (z coordinate of the point b on the separatrix) is the root of the Eq. (7) for the given values of  $\beta$ , F and  $\lambda$ . The coordinate of the second critical point C ( $z_c$ , 0), can be found by solving the following equation:

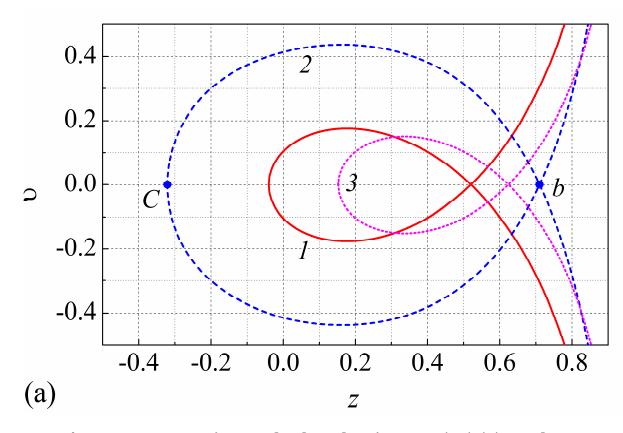
$$2F(z-b) - (z^2 - b^2) - \frac{\beta}{2}(z^4 - b^4) + \frac{2\lambda}{(1-z)} - \frac{2\lambda}{(1-b)} = 0.$$
 (14)

Using Eqs. (12)–(14), it is possible to calculate the magnitude of the oscillations range  $|z_b - z_c|$ , which is the range of the movable electrode controlled displacement at the specified MEMS parameters  $\beta$  and F, and for initial conditions  $z_{\text{init}}$ ,  $v_{\text{init}}$  and  $\lambda$ .

The numbers of the curves marked in Fig. 12 correspond to those shown in Fig. 2(a). It should be noted that the parameters of these MEMS are not located in the region bounded by the curves  $F_{\text{max}}$  and  $F_{\text{min}}$  (Fig. 5), and there is only one point of unstable equilibrium on their quasi-static dependences  $z(\lambda)$ .

The analysis of Eq. (12) and Fig. 12(a) shows that in this case, when the MEMS parameters change, only quantitative changes are observed: separatrices shift along z-axis while maintaining the shape; while both the area of the phase plane bounded by the separatrix and the oscillation amplitude vary.

Figure 13(a) shows the integral curves calculated for MEMS with parameters corresponding to the separatrix 2 in Fig. 12(a) under different initial conditions ( $z_{\text{init}}$ ,  $v_{\text{init}}$ ). The following values of  $z_{\text{init}}$  and  $v_{\text{init}}$  were used during the calculations: for curve 1 (0.710212, 0), for curve 2 (0.5, 0), for curve 3 (0.35, 0), for curve 4 (0.03, 0.12248), for curve 6 (-0.35, 0), and for curve 5 (0.73, 0). Corresponding time dependences of the movable electrode displacement for these integral curves are shown in Fig. 13(b).



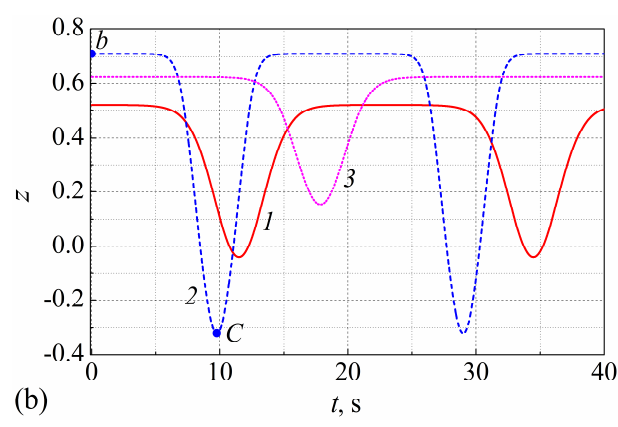


Fig. 12. Separatrices calculated using Eq. (12) (a), and corresponding time dependences of the movable electrode displacement (b).



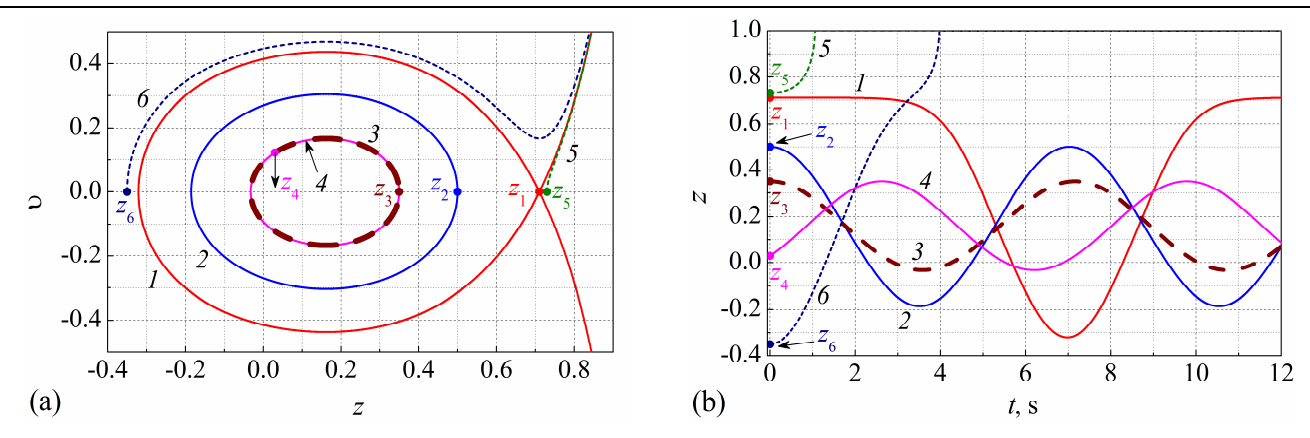


Fig. 13. Integral curves calculated using Eq. (11) under different initial conditions for MEMS with the following parameters  $\beta$  = 2, F = 0,  $\lambda$  = 0.119808 (a); corresponding time dependences of the movable electrode displacement calculated under different initial conditions (b).

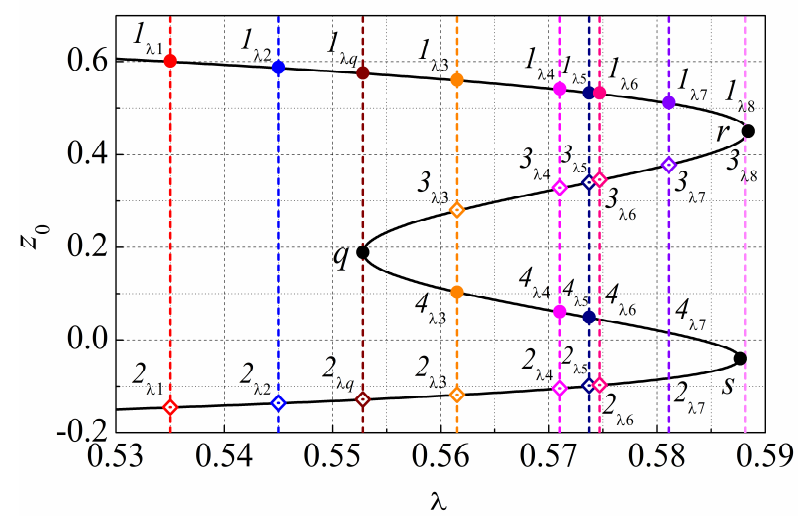


Fig. 14. The dependence of the static equilibrium position  $z_0$  versus the dimensionless voltage  $\lambda$ .

The analysis of Eq. (12) also shows that if the MEMS parameters  $\beta$  and F are in the region bounded by  $F_{max}$  and  $F_{min}$  curves (Fig. 5), and a second point of unstable equilibrium appears on their quasi-static dependences  $z(\lambda)$ , then when the initial parameters change, not only quantitative but also qualitative changes can be observed for the behavior of the system.

Figure 14 shows a fragment of the dependence  $z_0(\lambda)$  calculated for MEMS with parameters  $\beta=10$  and F=-0.584 shown in Fig. 2(b) (curve 2), located under quasi-static excitation within the region between the curves  $F_{max}$  and  $F_{min}$  (Fig. 5). In this case, four regions can be distinguished based on the dependence  $z_0(\lambda)$ : the first – where  $0 \le \lambda \le \lambda_q$ , the second – where  $\lambda_q < \lambda \le \lambda_s$ , the third – where  $\lambda_s < \lambda \le \lambda_r$  and the fourth – where  $\lambda_r < \lambda$ . Here  $\lambda_i$  are the heights of the applied voltage steps corresponding to the points q, s and r in Fig. 14, in our case  $0 < \lambda_q < \lambda_s < \lambda_r$ . The numbers indicate the positions of the characteristic representing points (Figs. 14, 15 and 17).

Figure 15 shows the separatrices calculated for MEMS parameters, which are located in the first region during the startup, where  $0 \le \lambda \le \lambda_q$ . It can be seen that as the value of  $\lambda$  increase, the area covered by the separatrix loop, the coordinate of the point z=b (circles 1.1) corresponding to the maximum permissible distance between the electrodes, as well as the permissible amplitude of oscillations decrease. The maximum permissible displacement velocities of the movable electrode (rhombuses  $2x_1$ ) are also reduced (including the velocities at the moment of startup). It should be noted that z coordinates of the points with the same name in Fig. 14 (ordinate axis) and in Fig. 15 (abscissa axis) coincide.

Figure 16 shows the time dependences of the movable electrode displacement calculated at the same  $\beta$ , F and  $\lambda$  as the separatrices shown in Fig. 15, and with the initial conditions ( $z_{\text{init}} = 0.99999z_{\text{cr}}$ ,  $v_{\text{init}} = 0$ ). Here  $z_{\text{cr}}$  is z coordinate of point b of the corresponding separatrix (abscissas of points  $1_{\lambda 1}$ ,  $1_{\lambda 2}$  and  $1_{\lambda 3}$  in Fig. 15). The curve numbers in Fig. 16 correspond to the curve numbers shown in Fig. 15. In order to observe oscillations and avoid pull-in effect the value of  $z_{\text{init}}$  was chosen less than  $z_{\text{cr}}$  as the initial conditions.

In general, the dependences for pulsed excitation corresponding to the first region, where  $0 \le \lambda \le \lambda_q$ , are similar to the dependences shown in Figs. 12 and 13. However, in this case, as the  $\lambda$  increases, the separatrices tend to have a second maximum.

The second maximum is clearly visible at separatrices when the MEMS parameters are in the second region (Fig. 14), where  $\lambda_q < \lambda \le \lambda_s$ . Figures 17(a) and 17(b) show such separatrices calculated for MEMS, which parameters  $\beta$  and F are located in the region bounded by the curves  $F_{\text{max}}$  and  $F_{\text{min}}$ : a) b = 0.56,  $\lambda = 0.56147097$  (curve 1); b = 0.54,  $\lambda = 0.57103222$  (curve 2); b = 0.533276,  $\lambda = 0.57372925$  (curve 3); b) b = 0.5325,  $\lambda = 0.57402422$  (curve 4); b = 0.5306,  $\lambda = 0.57473239$  (curve 5); b = 0.51,  $\lambda = 0.58116445$  (curve 6); b = 0.45,  $\lambda = 0.58843812$  (curve 7). It can be seen that as the value of  $\lambda$  increases, the area covered by the separatrix loop and the ordinate z = b decrease, then the separatrix is divided into two asymmetric regions (curves 4 and 5) – one for positive and the other for negative z. Further increase of  $\lambda$  leads to the appearance of one simply connected region (curve 6 in Fig. 17(b)), and then (for  $\lambda_s < \lambda \le \lambda_r$ ) to the contraction of the region bounded by the separatrix to a point (curve 7 in Fig. 17(b)), i.e., to the disappearance of the initial parameters, when the periodic oscillations are possible in this system. In the fourth area  $\lambda_r < \lambda$ , periodic oscillations are also not possible.



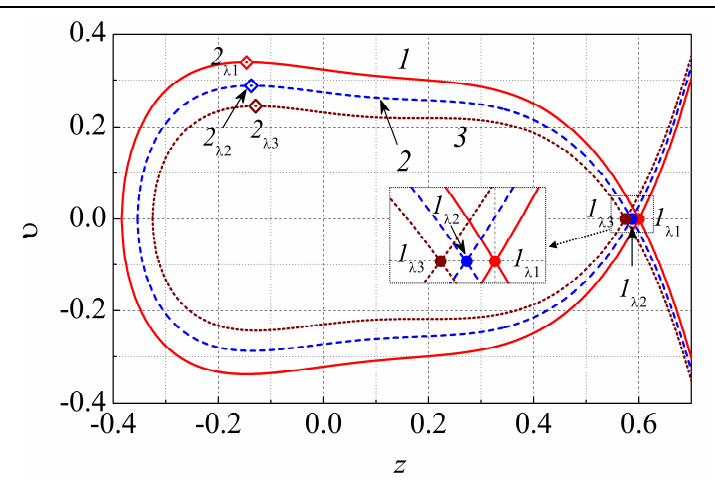


Fig. 15. Separatrices calculated for MEMS with  $\beta$  = 10 and F = -0.584, which are located in the region with  $0 \le \lambda \le \lambda_q$ .

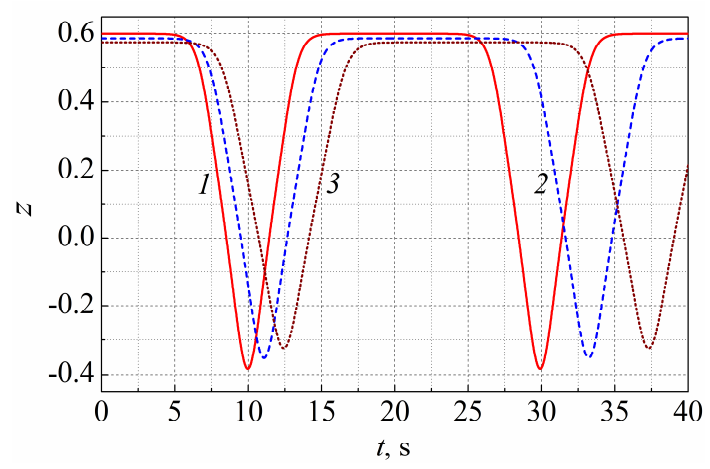


Fig. 16. Time dependences of the movable electrode displacement corresponding to the separatrices shown in Fig. 15.

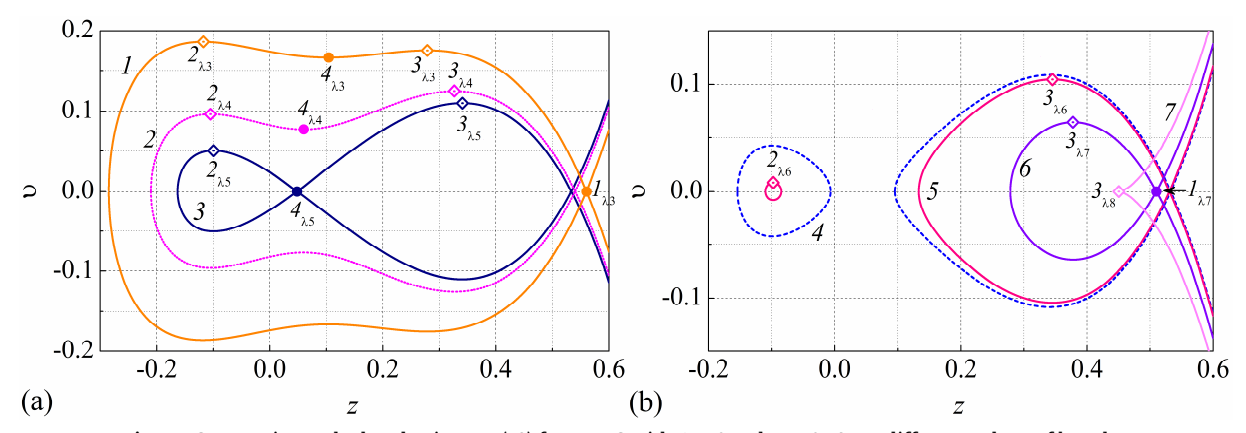


Fig. 17. Separatrices calculated using Eq. (12) for MEMS with  $\beta$  = 10 and F = -0.584 at different values of b and  $\lambda$ .

Time dependences of the movable electrode displacement corresponding to the integral curves shown in Fig. 17 are given in Fig. 18. It can be seen from Fig. 18(b), in particular, that in the region of the initial parameters where the separatrix is divided into two asymmetric simply connected regions (curves 4 and 5) depending on the initial parameters, oscillations will mainly focus either with positive or negative displacement of the movable electrode. It is also clear that a further increase of  $\lambda$  (curve 6) will lead to a concentration of oscillations in the region only with positive displacement of the movable electrode.

The characteristic points of the curves in Fig. 17 can be compared with the characteristic points shown in Fig. 14. The comparison shows that the circles  $1_{3i}$  correspond to the points b (determining the maximum allowable distance between the electrodes), and the circles  $4_{3i}$  correspond to the minimum points at the separatrices. In turn, the rhombuses  $2_{3i}$  and  $3_{3i}$  correspond to the points that determine the maximum permissible velocities and the corresponding displacements of the movable electrode during the system startup. The comparison of these points is shown in more detail in Fig. 19.

From all the variety of initial conditions, the case of the oscillations represents a particular interest, when at the moment of the electric voltage step application, the displacement of the movable electrode and its velocity are zero (zero initial conditions). Obviously, in this case, it is necessary that the point (0, 0) of the phase plane belongs to the region bounded by the separatrix loop.



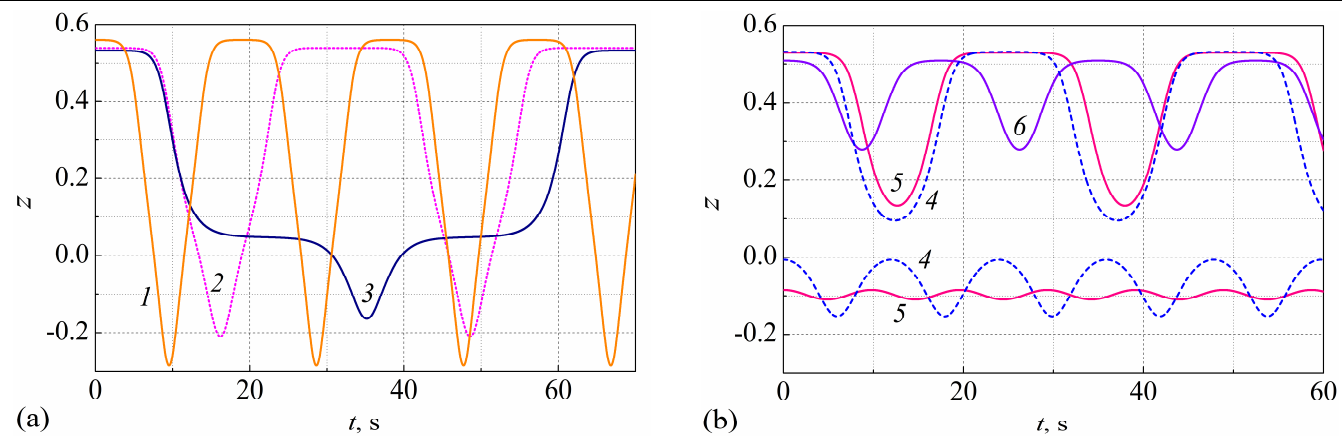


Fig. 18. Time dependences of the movable electrode displacement for MEMS with  $\beta$  = 10 and F = -0.584 calculated at different values of b and  $\lambda$ .

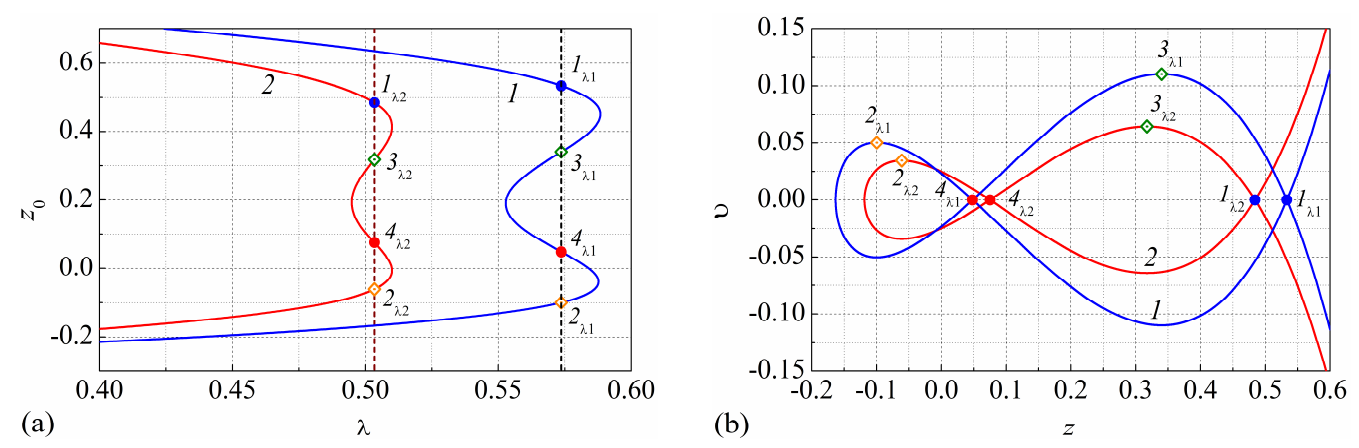


Fig. 19. The dependences of the static equilibrium position  $z_0$  on the magnitude of the dimensionless voltage  $\lambda$  (a), and the corresponding separatrices (b) obtained for MEMS with  $\beta$  = 10 and F = -0.584 (curves 1), and for  $\beta$  = 7.91 and F = -0.51 (curves 2).

The analysis shows that during plotting such separatrix for MEMS with F > -0.5 Eq. (12) must be used. Where the value of parameter b must be calculated using the following equation:

$$b(\beta, F) = A(\beta, F) - \left(\frac{1}{3\beta} - \frac{1}{16}\right) \frac{1}{A(\beta, F)} + \frac{1}{4},\tag{15}$$

where

$$A(\beta,F) = \sqrt[3]{\frac{F}{2\beta} + \frac{1}{8\beta} + \frac{1}{64} + \sqrt{\frac{2F+1}{128\beta} + \frac{F+2F^2}{8\beta^2} - \frac{1}{192\beta^2} + \frac{1}{27\beta^3}}}.$$

The resulting value of b will determine the maximum possible range of oscillations and, after its substitution into Eq. (13), also the maximum allowable value of the applied voltage  $\lambda$ .

Figure 20(a) shows the separatrices calculated using Eqs. (12) and (15) for MEMS with F > -0.5:  $\beta = 10$ , F = 0.3, b = 0.75742,  $\lambda = 0.282608$  (curve 1);  $\beta = 6$ , F = -0.1, b = 0.65126,  $\lambda = 0.29293$  (curve 2);  $\beta = 2$ , F = -0.1, b = 0.5241,  $\lambda = 0.20655$  (curve 3);  $\beta = 2$ , F = -0.3, b = 0.26997,  $\lambda = 0.32473$  (curve 4), whereas Fig. 20(b) shows the corresponding time dependences of the movable electrode displacement.

It can be seen from Fig. 20 that at F > -0.5 all separatrices include the point (0, 0), and they are located in the region of positive displacement z and all oscillations are also concentrated in the region with positive z. The areas bounded by the separatrix loop, the maximum permissible displacements of the movable electrode and the permissible range of oscillations decrease as the value of F decreases, but the period of oscillations increases. Calculations show that at F = -0.5, the area bounded by the separatrix shrinks to a point, and the oscillations stop.

A further decrease of F will lead to increase of the area bounded by the separatrix loop and the maximum allowable displacement of the movable electrode from the initial value.

The analysis shows that during plotting the separatrix for MEMS with F < -0.5 and with zero initial conditions, the following equation can be used

$$v = \pm \sqrt{z^2 \left[ \frac{2F}{z - 1} - 1 - \frac{\beta}{2} z^2 \right]}.$$
 (16)

In this case, the value of the maximum allowable displacement of the movable electrode  $z_C$  (the leftmost point of the separatrix) can be found as the real root of Eq. (17):

$$z^{3} - z^{2} + \frac{2}{\beta}z - 2\frac{2F + 1}{\beta} = 0.$$
 (17)



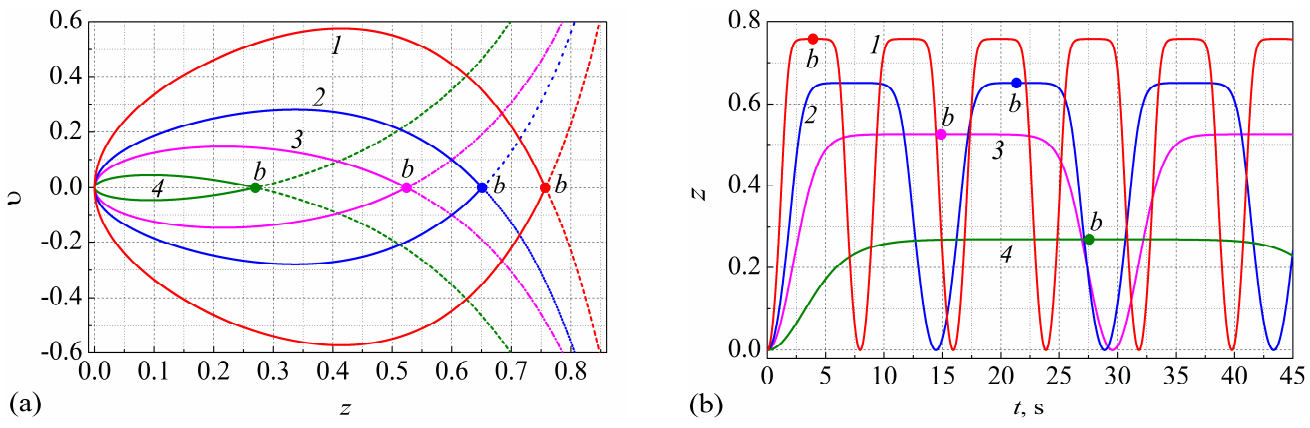


Fig. 20. Separatrices calculated using Eq. (12) for MEMS with F > -0.5 (a), and corresponding time dependences of the movable electrode displacement (b).

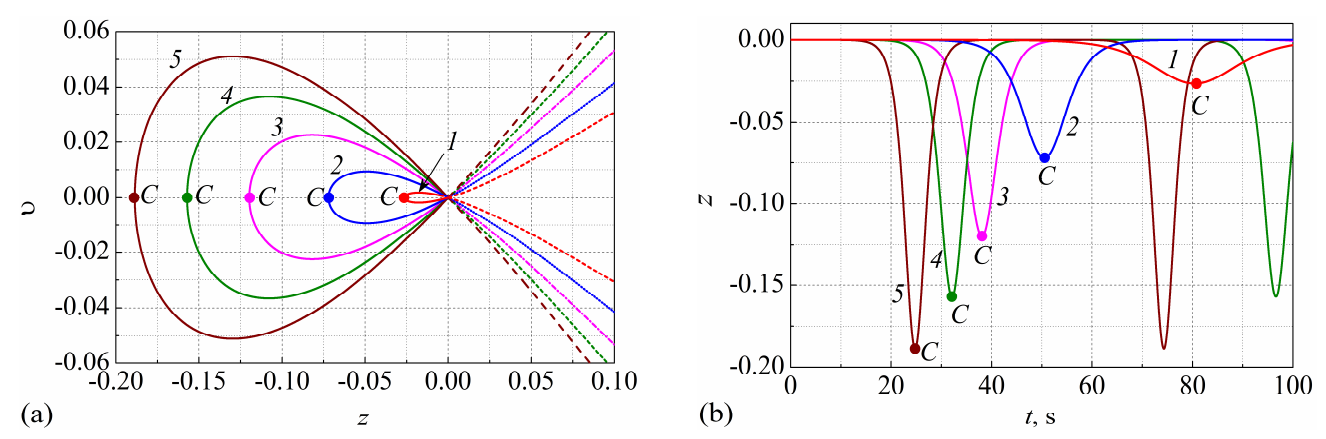


Fig. 21. Separatrices calculated using Eq. (16) for MEMS with  $\beta$  = 10 and different values of F (a), and time dependences of the movable electrode displacement corresponding to the presented separatrices (b).

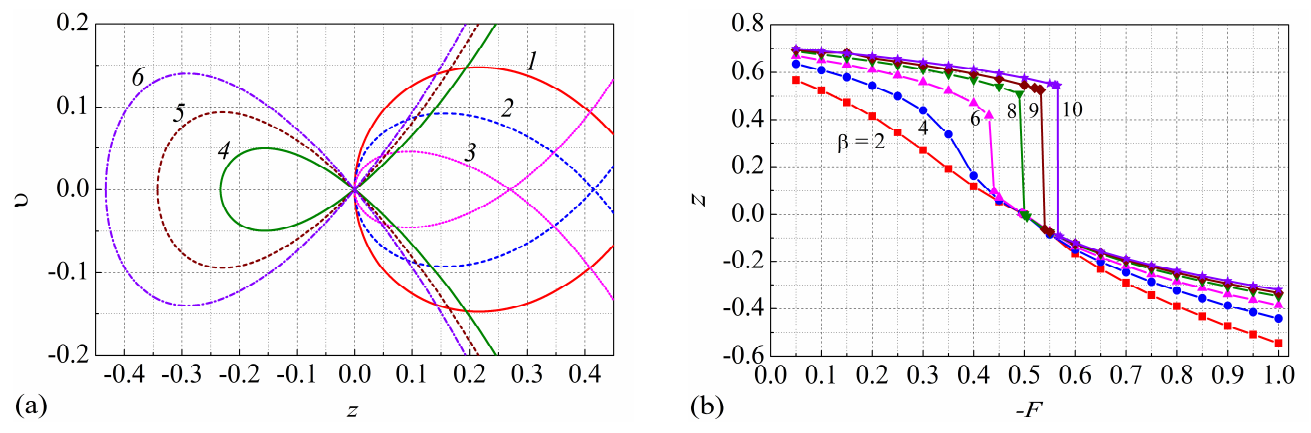


Fig. 22. Separatrices calculated for MEMS with  $\beta$  = 2 and different values of F (a), and the dependences of the maximum permissible controlled value of the movable electrode displacement z relative to the initial state versus the value of –F (b).

Figure 21(a) shows the separatrices calculated using Eq. (16) for MEMS with  $\beta$  = 10 and F < -0.5: F = -0.515 (curve 1); F = -0.55 (curve 2); F = -0.6 (curve 3); F = -0.65 (curve 4); F = -0.7 (curve 5), whereas Fig. 21(b) shows the corresponding time dependences of the movable electrode displacement.

The analysis shows that as the value of  $\beta$  decreases, the area bounded by the separatrix loop and  $|z_c|$  increase. Note that for MEMS with F < -0.5, the oscillations span is  $|z_c|$ , and the maximum allowable value of the applied voltage is  $\lambda_{cr} = -F$ .

Figure 22(a) demonstrates separatrices showing the transition from oscillations concentrated in the region of positive displacements to oscillations concentrated in the region of negative displacements, these separatrices have been obtained at  $\beta$  = 2 and different values of F: F = -0.1 (curve 1); F = -0.2 (curve 2); F = -0.3 (curve 3); F = -0.65 (curve 4); F = -0.75 (curve 5); F = -0.85 (curve 6). Figure 22(b) shows the dependences of the maximum permissible controlled value of the movable electrode displacement z relative to the initial state with z = 0 versus the value of the constant force F for different values of  $\beta$ . It can be seen that a change of the constant force F can significantly affect the magnitude of the movable electrode maximum displacement from the initial position for the two-electrode MEMS. For example, at F = -0.4 the value of the maximal achievable controlled displacement of the movable electrode from the initial position and, consequently, the range of the oscillations and the capacitance modulation depth due to the change of  $\beta$  from 2 to 10 can be increased by almost six times.

In order to determine whether two-electrode MEMS with the comb structure of electrodes and a split fixed electrode will be stable under dynamic (step-like) behavior of the electric voltage change and under arbitrary initial conditions, it is necessary to



obtain an appropriate separatrix. In this case, taking into account Eq. (8) and the symmetry of the problem, the separatrix equation can be represented as:

$$v^{2} = \left[ \frac{(1 - b^{2})(1 + \beta b^{2})}{(1 - z^{2})} - 1 - \frac{\beta}{2}(z^{2} + b^{2}) \right] (z^{2} - b^{2}).$$
 (18)

If initially (according to the technical specification for the MEMS parameters) the value of the required maximum displacement of the movable electrode (the value of b) is known, then using Eq. (18) it is possible to obtain the corresponding separatrix and determine the range of acceptable initial conditions, when the system will remain controllable. The acceptable value of  $\lambda$  in this case can be found by substituting of b instead of  $z_0$  in Eq. (9).

If the value of b is initially unknown, but the necessary value of  $\lambda$  is known, then the acceptable value of b can be found using Eq. (19):

$$|b| = \sqrt{\frac{1}{6\beta} \left[ 4\beta - 2 - A - \frac{\beta^2 + 2\beta + 1}{A} - i\frac{\sqrt{3}}{A} (A^2 - \beta^2 - 2\beta - 1) \right]},$$
(19)

where

$$A = \sqrt[3]{-\beta^3 - 3\beta^2 - 3\beta + 54\beta^2\lambda - 1 + 6\beta\sqrt{-3\lambda(\beta^3 + 3\beta^2 + 3\beta - 27\beta^2\lambda + 1)}}.$$

The analysis of Eq. (18) shows that for a given value of  $\lambda$  the changes of the separatrices for various  $\beta$  ( $\beta \le 2$ ) are only quantitative. In this case, the area covered by the separatrix loop and the maximum ordinates of the separatrix increase with increasing of  $\beta$ .

At the same time for  $\beta$  > 2 the changes of separatrices for various  $\beta$  are already qualitative. Figure 23 shows the separatrices calculated using Eq. (18) for  $\beta$  = 5 and several values of  $\lambda$ :  $\lambda$  = 0.275 (curve 1);  $\lambda$  = 0.287 (curve 2);  $\lambda$  = 0.305 (curve 3);  $\lambda$  = 0.30625 (curve 4); and  $\lambda$  = 0.31 (curve 5).

It can be seen from Fig. 23 that for  $\beta > 2$  as the value of  $\lambda$  increases the separatrix eventually splits into two symmetrical simply connected regions. Such simply connected separatrices limit the regions of periodic oscillations, where the displacement of the movable electrode does not change its sign.

If the value of the required maximum displacement of the movable electrode (the value of b) is initially known, then after dividing the separatrices into two simply connected regions, the values of the minimum displacement of the movable electrode according to Eq. (18) can be determined as

$$Z_{\rm c} = \pm \frac{1}{\beta} \sqrt{-\beta (2\beta b^2 - \beta + 2)}.$$
 (20)

Figure 24 shows the time dependence of the movable electrode displacement calculated using Eq. (8) at  $\beta$  = 5, and different values of  $\lambda$  and  $z_{init}$ :  $\lambda$  = 0.275,  $z_{init}$  = 0.623 (curve 1);  $\lambda$  = 0.305,  $z_{init}$  = 0.551 (curve 2);  $\lambda$  = 0.31,  $z_{init}$  = 0.533 (curve 3);  $\lambda$  = 0.31,  $z_{init}$  = -0.533 (curve 4); and  $\lambda$  = 0.30625,  $z_{init}$  = -0.54772 (curve 5). The calculations were performed at  $v_{init}$  = 0, but  $z_{init}$  ≠ 0. Moreover, for each pair of  $\beta$  and  $\lambda$  in order to maintain the oscillatory mode, the value of  $z_{init}$  was chosen to be slightly lower than the value of |b| calculated using Eq. (19). It is clear from Fig. 24 that as the value of  $\lambda$  increases the shape of oscillations differ more and more from the harmonic ones, and when  $\lambda$  ≥ 0.03125( $\beta$  + 2)<sup>2</sup>/ $\beta$  depending on the values of  $z_{init}$  the oscillations are localized either in the region of positive (curve 3) or negative (curve 4) displacements.

In the case when for two-electrode MEMS with a comb structure of electrodes there is a separatrix with one simply connected region, the oscillation period  $\tau_0$  can be determined without solving Eq. (8). Where:

$$\tau_0 = \int_a^b \frac{1}{v(y)} dy.$$

Figure 25 shows the dependences of the static equilibrium position  $z_0$  during quasi-static excitation of the system versus the magnitude of the dimensionless voltage  $\lambda$  for  $\beta=2$  and  $\beta=5$ . The arrows show the range of oscillations shown in Fig. 24, the numbers of the arrows correspond to the numbers of the curves in Fig. 24. This figure also shows with round markers the position of the maximum displacements of the movable electrode from the equilibrium position during the oscillations shown in Fig. 24 (dynamic excitation). Rhombs on quasi-static dependences indicate displacements of the movable electrode at which the maximum displacement velocity of the movable electrode will be achieved during dynamic excitation.

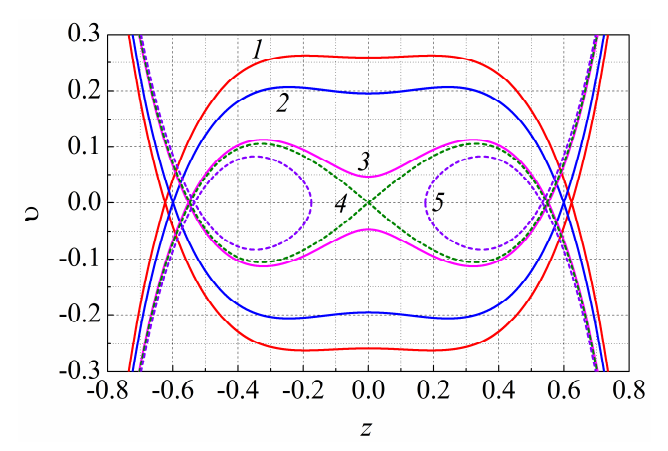


Fig. 23. Separatrices for MEMS with a comb structure of electrodes calculated using Eq. (18) at  $\beta$  = 5 and different values of  $\lambda$ .



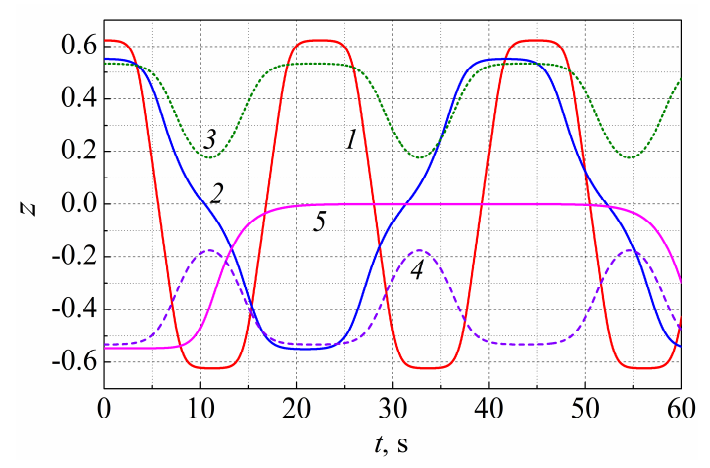


Fig. 24. Time dependences of the movable electrode displacement calculated using Eq. (8) for  $\beta$  = 5 and different values of  $\lambda$  and  $z_{init}$ .

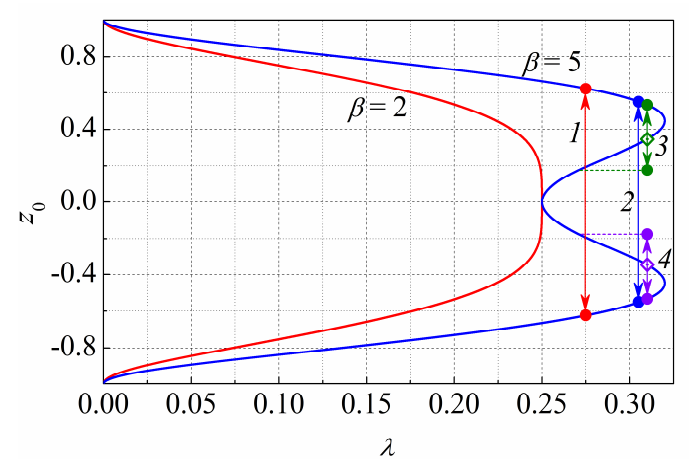


Fig. 25. Dependences of the static equilibrium position  $z_0$  versus the magnitude of the dimensionless voltage  $\lambda$  for  $\beta=2$  and  $\beta=5$ .

The analysis shows that for  $\lambda > 0.03125(\beta + 2)^2/\beta$  the modulus of the maximum movable electrode displacement  $|z_{max}|$  will not exceed  $1/\sqrt{2}$ , and the controlled capacitance modulation depth will not exceed 2, respectively. In cases when the MEMS parameters correspond to separatrices with a single simply connected region, the maximum achievable capacitance modulation depth (determined by the maximum allowable displacement of the movable electrode) increases when the value of  $\beta$  increases for a given value of  $\lambda$ .

If for two-electrode MEMS with a comb structure of electrodes not only a stationary but also a movable electrode is split, then even for the dynamic (stepwise, step-like) nature of the electric voltage change and arbitrary initial conditions, the results and conclusions of the corresponding analysis for two-electrode MEMS with a comb structure of electrodes and only a split fixed electrode can be used taking into account the replacement of  $\lambda$  by  $\lambda^* = n \cdot \lambda$ . At the same time, the value of  $V_{0,cr}$  will decrease by  $\sqrt{n}$  times. The decrease of permissible voltage occurs because as the number of the split electrode components increases the capacitance of the MEMS increases too. As a result, for a given value of electrical voltage the electrostatic force of attraction between the electrodes increases and the pull-in effect occurs at lower voltages.

The presented above equations and figures show the relationship between the quasi-static and dynamic characteristics of MEMS at specified system parameters.

#### 4. Conclusion

The study of the parameter influence of the two-electrode MEMS with interelectrode gap changing and their initial state immediately before the application of electric excitation on the operation of such systems has shown that:

- The nonlinear nature of the restoring elastic and electrostatic forces in the presence of an additional constant force, as well as the rate of the applied electrical voltage change can significantly modify the system behavior;
- The combination of these factors with quasi-static nature of the excitation can lead to the appearance of a second point of unstable equilibrium and hysteresis on the reverse dependences of the movable electrode displacement versus the applied voltage, and with the dynamic change of the applied electric voltage to the localization of the oscillations either in the region with positive or in the region with negative displacement;
- For MEMS with a comb structure of electrodes where not only the fixed, but also the movable electrode is split, the pull-in voltage decreases as the number of the split electrodes components increases;
- Due to the optimal use of the movable electrode weight in MEMS with a nonlinear dependence of the restoring force versus the movable electrode displacement, the capacitance modulation depth and the relative range of the controlled capacitance change can be increased by several times in comparison with MEMS having a linear dependence of the restoring force.

In general, the obtained analytical expressions can significantly reduce the search time for necessary and acceptable parameters of two-electrode MEMS during the preliminary design stage.



#### **Author Contributions**

V.P. Dragunov planned the study, initiated the project, and suggested the mathematical model; D.I. Ostertak developed the mathematical model, analyzed the results, and examined the theory validation; E.V. Dragunova carried out the literature survey; M.A. Kuznetsov carried out the calculations. The manuscript was written through the contribution of all authors. All authors discussed the results, reviewed, and approved the final version of the manuscript.

## Acknowledgments

The authors thank Professor Kibis O.V. for valuable comments and suggestions made in the course of this work. The study was carried out using the equipment of the educational design centre for power electronics of Novosibirsk State Technical University.

#### **Conflict of Interest**

The authors declared no potential conflicts of interest concerning the research, authorship, and publication of this article.

# **Funding**

The study is supported by the Ministry of Science and Higher Education of the Russian Federation (project FSUN-2023-0006).

# **Data Availability Statements**

The datasets generated and/or analyzed during the current study are available from the corresponding author on reasonable request.

#### Nomenclature

Nomenciature		
Components of the cubic equation solution	Z	Relative displacement of the movable electrode
Maximum permissible controlled distance between the movable and fixed electrodes	$Z_b$	Relative displacement of the movable electrode corresponding to the special point $\boldsymbol{b}$
Second critical point	Zc	Relative displacement of the movable electrode corresponding to the second critical point ${\cal C}$
Parallel-plate capacitance [F]	$Z_{cr,}Z_{cr,i}$	Critical relative displacement of the movable electrode
Maximal capacitance of the variable capacitor [F]	$z_{init}$	Normalized initial displacement of the movable electrode
Minimal capacitance of the variable capacitor [F]	$Z_{\text{max}}$	Maximum movable electrode displacement for MEMS with comb structure
Initial gap between the electrodes [m]	$\alpha$	Angle between the direction of the normal to the movable electrode surface and the direction of the external force [rad]
Normalized projection of the constant force	$\beta$	The normalized coefficient of nonlinearity
Constant external force [N]	$\varepsilon$	Relative permittivity of the gas within the interelectrode gap
Projection of F <sub>0</sub> to the surface normal [N]	$arepsilon_0$	Permittivity of free space [F/m]
Maximal value of the force when two maxima are observed	$\eta$	Capacitance modulation depth
Minimal value of the force when two maxima are observed	$\eta_{d}$	Relative range of the controlled capacitance change
The linear spring constant [N/m]	$\eta_{max}$	Maximum achievable capacitance modulation depth
Cubic nonlinearity of the restoring force [N/m <sup>3</sup> ]	$\eta_{d,\max}$	Maximum relative range of the controlled capacitance change
Mass of the movable electrode [kg]	$\lambda$ , $\lambda_i$	Dimensionless voltage
Number of components of the split electrode	$\lambda_{ m cr,}\lambda_{ m cr,i}$	Critical dimensionless voltage
Area of the electrode overlap [m²]	$\lambda^*$	Dimensionless voltage in case of split electrodes
Time [s]	au	Normalized time
Voltage between the movable and stationary electrodes [V]	$ au_0$	Normalized period of oscillations for MEMS with comb structure
Critical voltage (pull-in voltage) [V]	υ	Normalized velocity of the movable electrode
Movable electrode displacement [m]	$v_{ m init}$	Normalized initial velocity of the movable electrode
Integration variable	$\omega_0$	Natural vibration frequency [s <sup>-1</sup> ]
	Maximum permissible controlled distance between the movable and fixed electrodes Second critical point  Parallel-plate capacitance [F] Maximal capacitance of the variable capacitor [F] Minimal capacitance of the variable capacitor [F]  Initial gap between the electrodes [m]  Normalized projection of the constant force Constant external force [N] Projection of F <sub>0</sub> to the surface normal [N]  Maximal value of the force when two maxima are observed  Minimal value of the force when two maxima are observed The linear spring constant [N/m] Cubic nonlinearity of the restoring force [N/m²]  Mass of the movable electrode [kg] Number of components of the split electrode Area of the electrode overlap [m²] Time [s] Voltage between the movable and stationary electrodes [V] Critical voltage (pull-in voltage) [V] Movable electrode displacement [m]	Components of the cubic equation solution  Maximum permissible controlled distance between the movable and fixed electrodes  Second critical point  Zc  Parallel-plate capacitance [F]  Maximal capacitance of the variable capacitor [F]  Minimal capacitance of the variable capacitor [F]  Initial gap between the electrodes [m]  Normalized projection of the constant force  Constant external force [N]  Projection of $F_0$ to the surface normal [N]  Maximal value of the force when two maxima are observed  Minimal value of the force when two maxima are observed  The linear spring constant [N/m]  Cubic nonlinearity of the restoring force [N/m³]  Mass of the movable electrode [kg]  Number of components of the split electrode  Area of the electrode overlap [m²]  Time [s]  Voltage between the movable and stationary electrodes [V]  Critical voltage (pull-in voltage) [V]  Movable electrode displacement [m]

#### References

- [1] Bustillo, J.M., Howe, R.T., Muller, R.S., Surface micromachining for microelectromechanical systems, Proceedings of the IEEE, 86, 1998, 1552-1574.
- [2] Batra, R.C., Porfiri, M., Spinello, D., Review of modeling electrostatically actuated microelectromechanical systems, Smart Materials and Structures, 16, 2007, R23–R31.
- [3] Tang, W.C., Nguyen, T.-C.H., Howe, R.T., Laterally Driven Polysilicon Resonant Microstructures, Sensors and Actuators, 20, 1989, 25-32.
- [4] Dean, R.N., Luque, A., Applications of Microelectromechanical Systems in Industrial Processes and Services, IEEE Transactions on Industrial Electronics, 56, 2009,
- [5] Eom, K., Park, H.S., Yoon, D.S., Kwon, T., Nanomechanical resonators and their applications in biological/chemical detection: Nanomechanics principles, Physics Reports, 503, 2011, 115–163.
- [6] Zhang, W.-M., Meng, G., Nonlinear Dynamic Analysis of Electrostatically Actuated Resonant MEMS Sensors Under Parametric Excitation, IEEE Sensors Journal,
- [7] Chuang, W.-C., Lee, H.-L., Chang, P.-Z., Hu, Y.-C., Review on the Modeling of Electrostatic MEMS, Sensors, 10, 2010, 6149–6171. [8] Oh, K.W., Ahn, C.H., A review of microvalves, Journal of Micromechanics and Microengineering, 16, 2006, R13–R39.
- [9] Nisar, A., Afzulpurkar, N., Mahaisavariya, B., Tuantranont, A., MEMS-based micropumps in drug delivery and biomedical applications, Sensors and Actuators



[10] (Rich) Pryputniewicz, R.J., Progress in Microelectromechanical Systems, Strain, 43, 2007, 13-25.

[11] Liu, D.K.-C., Friend, J., Yeo, L., A brief review of actuation at the micro-scale using electrostatics, electromagnetics and piezoelectric ultrasonics, Acoustical Science and Technology, 31, 2010, 115–123.

[12] Loh, O.Y., Espinosa, H.D., Nanoelectromechanical contact switches, Nature Nanotechnology, 7, 2012, 283–295.

- [13] Zhang, L., Zhang, H., Li, X., Qiao, N., Gao, X., Ji, Y., The Nonlinear Dynamics of a MEMS Resonator with a Triangular Tuning Comb, Micromachines, 14, 2023, 2109.
- [14] Liu, Z., Qin, B., Shi, Z., Wang, X., Lv, Q., Wei, X., Huan, R., Nonlinearity-Induced Asymmetric Synchronization Region in Micromechanical Oscillators, Micromachines, 15, 2024, 238.
- [15] Shaikh, F.K., Zeadally, S., Energy harvesting in wireless sensor networks: A comprehensive review, Renewable and Sustainable Energy Reviews, 55, 2016, 1041-1054
- [16] Khan, F.U., Qadir, M.U., State-of-the-art in vibration-based electrostatic energy harvesting, *Journal of Micromechanics and Micromegineering*, 26, 2016, 103001. [17] Dragunov, V.P., Ostertak, D.I., Pelmenev, K.G., Sinitskiy, R.E., Dragunova, E.V., Load resistance influence on the Bennet doubler based electrostatic mechanical-to-electrical energy converter operation, *Sensors and Actuators A: Physical*, 351, 2023, 114162.
- [18] Zhang, W.-M., Yan, H., Peng, Z.-K., Meng, G., Electrostatic pull-in instability in MEMS/NEMS: A review, Sensors and Actuators A: Physical, 214, 2014, 187–218.

- [19] Nathanson, H.C., Newell, W.E., Wickstrom, R.A., Davis, J.R., The resonant gate transistor, IEEE Transactions on Electron Devices, 14, 1967, 117–133.
  [20] The coalescence of closely spaced drops when they are at different electric potentials, Proceedings of the Royal Society of London. Series A, 306, 1968, 423–434.
- [21] Luo, A.C.J., Wang, F.Y., Chaotic motion in a micro-electro-mechanical system with non-linearity from capacitors, Communications in Nonlinear Science and Numerical Simulation, 7, 2002, 31–49.
- [22] Bochobza-Degani, O., Nemirovsky, Y., Experimental Verification of a Design Methodology for Torsion Actuators Based on a Rapid Pull-In Solver, Journal of Microelectromechanical Systems, 13, 2004, 121–130. [23] Zhang, Y., Zhao, Y., Numerical and analytical study on the pull-in instability of micro-structure under electrostatic loading, Sensors and Actuators A: Physical,
- 127, 2006, 366–380.
- [24] Rokni, H., Seethaler, R.J., Milani, A.S., Hosseini-Hashemi, S., Li, X.-F., Analytical closed-form solutions for size-dependent static pull-in behavior in electrostatic micro-actuators via Fredholm integral equation, Sensors and Actuators A: Physical, 190, 2013, 32–43.
  [25] Mirkalantari, S.A., Hashemian, M., Eftekhari, S.A., Toghraie, D., Pull-in instability analysis of rectangular nanoplate based on strain gradient theory considering surface stress effects, Physica B: Condensed Matter, 519, 2017, 1–14.
- [26] Kumar, M., Mukherjee, B., Sen, S., Analysis of static charge induced pull-in of an electrostatic MEMS, Communications in Nonlinear Science and Numerical Simulation, 96, 2021, 105690.
- [27] Shang, H., Pull-in instability of a typical electrostatic MEMS resonator and its control by delayed feedback, Nonlinear Dynamics, 90, 2017, 171–183.
- [28] Abdelraouf, M.E., Kandil, A., Zahra, W.K., Elsaid, A., Analyzing MEMS resonator static pull-in and dynamics under electric excitation via position feedback controller, Physica Scripta, 100, 2025, 0152a2.
- [29] Bolotin, V.V., Dynamic Instabilities in Mechanics of Structures, Applied Mechanics Reviews, 52, 1999, R1–R9.
  [30] Fang, Y., Li, P., A new approach and model for accurate determination of the dynamic pull-in parameters of microbeams actuated by a step voltage, Journal of Micromechanics and Microengineering, 23, 2013, 045010.
- [31] Fargas-Marques, A., Casals-Terre, J., Shkel, A.M., Resonant Pull-In Condition in Parallel-Plate Electrostatic Actuators, Journal of Microelectromechanical Systems, 16, 2007, 1044–1053.
- [32] Alsaleem, F.M., Younis, M.I., Ouakad, H.M., On the nonlinear resonances and dynamic pull-in of electrostatically actuated resonators, *Journal of Micromechanics and Microengineering*, 19, 2009, 045013.
  [33] Nayfeh, A.H., Younis, M.I., Abdel-Rahman, E.M., Dynamic pull-in phenomenon in MEMS resonators, *Nonlinear Dynamics*, 48, 2007, 153–163.
- [34] Zand, M.M., The Dynamic Pull-In Instability and Snap-Through Behavior of Initially Curved Microbeams, Mechanics of Advanced Materials and Structures, 19, 2012, 485-491.
- [35] Moghimi Zand, M., Ahmadian, M.T., Dynamic pull-in instability of electrostatically actuated beams incorporating Casimir and van der Waals forces, Proceedings of the Institution of Mechanical Engineers, Part C: Journal of Mechanical Engineering Science, 224, 2010, 2037–2047.
- [36] Sedighi, H.M., Size-dependent dynamic pull-in instability of vibrating electrically actuated microbeams based on the strain gradient elasticity theory, Acta Astronautica, 95, 2014, 111–123.
  [37] Dragunov, V.P., Dragunova, E.V., Specific Features of MEM Systems' Functioning, Journal of Nano- and Microsystem Technique, 6, 2015, 43–52.
  [38] Dragunov, V.P., Dragunova, L.S., An influence of the mobile electrode weight on functioning MEMS, Proceedings of the RHEAS, 28, 2015, 50–60.

- [39] Saw, G.R., Singh, S., Chakraborty, G., Analysis of Pull-In Parameters of a Microelectromechanical Beam With van der Waals Force Using Modified Couple Stress Theory, Journal of Applied Mechanics, 92, 2025, 061007.
- [40] Shao, Y., Cui, Y., Mathematical approach for rapid determination of pull-in displacement in MEMS devices, Frontiers in Physics, 13, 2025, 1521849.
  [41] Yang, X., Kästner, P., Käkel, E., Smolarczyk, M., Liu, S., Li, Q., Hillmer, H., Study of Dynamics in Metallic MEMS Cantilevers—Pull-In Voltage and Actuation
- Speed, Applied Sciences, 13, 2023, 1118.
- [42] Skrzypacz, P.S., Putek, P.A., Pruchnik, B.Cz., Turganov, A., Ellis, G.A., Gotszalk, T.P., Analysis of dynamic pull-in for lumped MEMS model of atomic force microscope with constant magnetic excitation, *Journal of Sound and Vibration*, 617, 2025, 119215.
  [43] Zhu, Y., Shang, H., Jump and Pull-in Instability of a MEMS Gyroscope Vibrating System, *Micromachines*, 14, 2023, 1396.
- [44] Rast, S., Wattinger, C., Gysin, U., Meyer, E., Dynamics of damped cantilevers, Review of Scientific Instruments, 71, 2000, 2772–2775.
- [45] Yasumura, K.Y., Stowe, T.D., Chow, E.M., Pfafman, T., Kenny, T.W., Stipe, B.C., Rugar, D., Quality factors in micron- and submicron-thick cantilevers, Journal of Microelectromechanical Systems, 9, 2000, 117–125. [46] Nayfeh, A.H., Mook, D.T., Nonlinear oscillations, Wiley, 1995.
- [47] Ostertak, D., An analysis of electrostatic interactions in parallel-plate MEMS with regard to fringing field effects within a 3D-approach, Proceedings of the RHEAS, 34, 2017, 116–132.
- [48] Nemirovsky, Y., Bochobza-Degani, O., A methodology and model for the pull-in parameters of electrostatic actuators, Journal of Microelectromechanical Systems, 10, 2001, 601–615.
- [49] Dragunov, V.P., Ostertak, D.I., Operational Features of MEMS with an Even Number of Electrodes, Russian Microelectronics, 47, 2018, 393-406.
- [50] Andronov, A.A., Vitt, A.A., Hajkin, S.E., Theory of oscillations, Moscow: Nauka, 1981.

# ORCID iD

Valery P. Dragunov https://orcid.org/0000-0002-7088-5727 Dmitriy I. Ostertak https://orcid.org/0000-0003-2903-0732 Evgeniya V. Dragunova https://orcid.org/0000-0002-0677-9735 Maksim A. Kuznetsov https://orcid.org/0000-0003-3052-6647



© 2025 Shahid Chamran University of Ahvaz, Ahvaz, Iran. This article is an open access article distributed under the terms and conditions of the Creative Commons Attribution-NonCommercial 4.0 International (CC BY-NC 4.0 license) (http://creativecommons.org/licenses/by-nc/4.0/).

How to cite this article: Dragunov, V.P., Ostertak, D.I., Dragunova, E.V., Kuznetsov, M.A. Effect of Initial Conditions on the Behavior of Two-Electrode MEMS with Variable Interelectrode Gap, J. Appl. Comput. Mech., xx(x), 2025, 1-16. https://doi.org/10.22055/jacm.2025.48509.5291

Publisher's Note Shahid Chamran University of Ahvaz remains neutral with regard to jurisdictional claims in published maps and institutional affiliations.

